Low energy differential elastic electron scattering from acetonitrile (CH$_3$CN)

M. Zawadzki, and M. A. Khakoo

Low energy differential elastic electron scattering from acetonitrile (CH₃CN)

M. Zawadzki[1,2,a)] and M. A. Khakoo[1]

[1]*Department of Physics, California State University, Fullerton, California 92831, USA*
[2]*Atomic Physics Division, Department of Atomic, Molecular and Optical Physics, Faculty of Applied Physics and Mathematics, Gdańsk University of Technology, ul. G. Narutowicza 11/12, 80-233 Gdańsk, Poland*

Measurements of elastic differential cross sections for electron scattering from acetonitrile (CH₃CN) have been performed utilizing a crossed electron-molecular beam experiment and with the relative flow method, for the incident electron energy range of 0.7 eV–30 eV and the scattering angle range of 10°–130°. These differential cross sections have been used to calculate the elastic integral and momentum-transfer cross sections, revealing a π^* resonance located around 3 eV. The elastic differential cross sections are compared with available theoretical models using the R-matrix method and the Schwinger multichannel method. *Published by AIP Publishing.* https://doi.org/10.1063/1.5049810

I. INTRODUCTION

There has been considerable interest in low-energy electron interactions with gaseous molecular targets especially during the last several decades because of their fundamental importance in the physics, biology, and chemistry of plasmas.[1–6] Although the technological applications of cyanide containing molecules motivated the theoretical and experimental investigations of such targets, comprehensive and reliable sets of cross sections are still needed for understanding the physical chemistry of processes relevant to these molecules as well as providing input data for theoretical electron collision models.

Acetonitrile, also known as methyl cyanide, is one of the simplest organic nitriles. It has a methyl structure attached to a CN functional group via a carbon-carbon bond (see Fig. 1). This molecular species has been detected within the molecular cloud in an active star forming region Kleinmann-Low Nebula,[8] Titan's atmosphere,[9] and hot cores in molecular clouds.[10] Interestingly, the rotational transitions of methyl cyanide were proven to be a good tool to estimate the temperature and column density of hot molecular cores.[11–13]

Among the reports on acetonitrile, one can find experimental and theoretical studies of the ground-state electronic structure.[14] A combined electron transmission and inner-shell energy loss spectroscopy study also provided detailed information on excited states related to virtual orbitals within a molecular orbital model.[15] Also, investigations of resonant vibrational excitation,[16] absolute differential cross sections (DCSs),[17] and vibronic coupling in resonant selective vibrational excitation by electron impact,[19] as well as low energy electron attachment,[20,21] have been reported.

For a molecule such as acetonitrile, with a large permanent dipole moment, obtaining reliable integral cross sections (ICSs) is still challenging since the small-angle interpolation of the experimental differential cross section and different theoretical approximations used lead to large discrepancies between measured and calculated values. It has a dipole moment of 3.91 D,[22] which leads one to expect dominant long-range dipole interactions with impinging electrons[23–25] resulting in steeply raised forward-scattering cross sections.

Theoretical work on integral cross sections and differential cross sections for the elastic scattering of low-energy electrons by acetonitrile, using the Schwinger multichannel (SMC) method with pseudopotentials, was implemented by Maioli and Bettega.[26] Similar DCSs and ICSs were calculated by Fujimoto et al.,[27] but using available molecular R-matrix codes. These theoretical values of ICSs are in significant disagreement with each other, and presently there exists no available experimental electron collision data for acetonitrile that could shed light on these theoretical results to resolve any doubts as to which model is more accurate.

In this paper, we report experimental DCSs, ICSs, and momentum transfer cross sections (MTCSs) for electron scattering of acetonitrile in the incident electron energy (E_0) range of 0.7–30 eV and scattering angle (θ) in the range of 10°–130°.

II. METHOD

A. Experiment

The apparatus and procedure used in the reported experiment have been described in detail elsewhere, e.g., in the work of Khakoo et al.,[28] so only a brief summary will be given here.

The electrons were produced by a tungsten hairpin filament. To ensure a well-defined electron beam energy profile, the electron gun and electron analyzer were equipped
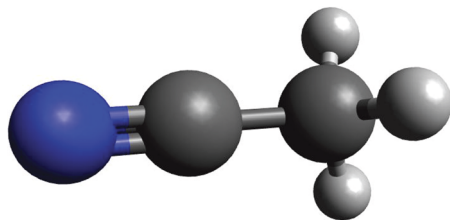
a)Electronic mail: mzawadzki@fullerton.edu

FIG. 1. Ball-and-stick model of the structure of acetonitrile, N≡C–CH₃, generated and optimized with Gaussian 09.[7]

with double 180° hemispherical energy selectors. The main components of the apparatus were made of titanium. Cylindrical electron optics guided electrons through the apertures made of molybdenum, and the system was kept at an elevated temperature of about 130 °C with a magnetically free biaxial heater.[29] By applying a double μ-metal shield on the inner walls of the vacuum chamber and utilizing a Helmholtz coil, the magnetic field in the collision region was reduced to ≈1 mG. The electron beam current was typically 18-26 nA, and the energy resolution of the electron beam was about 50 meV, full width at half maximum. The electron energy calibration was ensured by measuring the position of the signal minimum in elastic scattering of the 2^2S He⁻ resonance at E_0 = 19.366 eV at θ = 90°. The stability of the electron beam E_0 was better than 30 meV during a 24-h experimental run. The energy calibration yielded a contact potential which varied from 0.6 to 0.7 eV, and the power supply biasing the filament was appropriately corrected for this so as to provide the right energy for the electron beam. Detection of the scattered electrons was performed by a discrete dynode electron multiplier[30] which had a high dynamic range from ≈0.01 to 10^6 Hz.

In the crossed-beam arrangement, the target gas beam was formed by effusing the gas through a 0.4-mm-diameter aperture attached to the end of a 6.35-mm aluminum tube. The use of an aperture rather than a conventional tube or capillary-array source obviates the application of pressure ratios, dependent on the molecular diameter of gases used, within the relative flow method. The details of the relative-flow method with a collimating thin-aperture source used in this work are described in Ref. 31. The thin-aperture source was located ≈5 mm below the collision region and could be moved in and out of alignment with the electron beam, enabling an expedient and accurate determination of the electron-gas scattering background.[32]

The electron monochromator and analyzer were housed inside a vacuum chamber with a typical gas-off background pressure of 8×10^{-8} Torr and a gas-on pressure of around 2×10^{-6} Torr. The elastic electron scattering DCS for acetonitrile, $\mathcal{Q}_A(E_0, \theta)$, is obtained from the relative-flow formula

$$\mathcal{Q}_A(E_0, \theta) = \mathcal{Q}_{He}(E_0, \theta) \frac{\mathcal{R}_{He} \, I_{S,A}}{\mathcal{R}_A \, I_{S,He}} \sqrt{\frac{M_{He}}{M_A}}, \qquad (1)$$

where $\mathcal{R}$ stands for the relative flow rates, I_S represents the scattering rates, and M represents the molar masses where the subscripts indicate the gas species, with A being the unknown

gas (acetonitrile) whose DCS is to be determined and He being the standard gas (helium) whose DCSs are known. The measured acetonitrile DCSs were normalized to elastic DCSs for helium, which were taken from Refs. 33 and 34 and which are well established.

To ensure reproducibility, each experiment with acetonitrile and helium was taken usually twice or greater for reproducibility checking and then followed with weighted averaging of the datasets obtained. The sample of CH_3CN used was from Sigma-Aldrich and had a stated purity of 99.8%. Before measurement, acetonitrile was purified with repeated freeze-pump-thaw cycles at the liquid-N_2 temperature to remove dissolved air and other volatile impurities. For reference measurements, a commercially supplied sample of 4.5 grade He was used.

The uncertainties in DCSs may arise from several contributions, both statistical and systematic. When calculating the overall error for measured data, we included uncertainties in helium elastic DCSs (6%-8%), uncertainties in flow rates (2%-4%), statistical uncertainties in the signal + background and background (2%-10%), and standard deviation uncertainties in the reproducibility of multiple DCSs measurements (7%-8%). These are all added in quadrature to yield the overall errors which range from 12% to 18%.

B. DCS integration

In determining the ICSs, we have to take care as the dipole elastic DCSs are almost singular at small θ values. We have used the Born-dipole approximation (see, e.g., Ref. 36) to extrapolate our DCSs to θ = 0 and then integrated our DCSs over all solid angles. The error bars for this are estimated from this difference vs. extrapolating a flat DCSs approach, which results in a 15% to 20% error overall. We have discussed this at length in our earlier papers; see, e.g., Ref. 36 and the papers referenced therein. Briefly, the DCSs were extrapolated (closely following the Born-dipole shape at small θ) and a rough theoretical DCS shape at large θ using either Ref. 26 or 27 then integrating the extrapolated DCSs at all θ to obtain ICSs. The DCSs were also flat-extrapolated to small and large θ using the extreme experimental DCSs and integrated. The difference between the ICSs and the flat-extrapolated ICSs was considered as an additional error of the ICSs and added to its overall error in quadrature. This difference did not exceed 10%. The situation for MTCSs is better since it has the added $(1 - \cos \theta)$ factor.

III. RESULTS AND DISCUSSION

The normalized acetonitrile DCSs measured in this work plus the ICSs and MTCSs determined from them are listed in Table I along with 1 standard deviation error.

There are several energy points that allow direct comparison of the measured data with theory. Figure 2 compares the present experimental DCSs at selected E_0 values with the available calculations for acetonitrile found in the literature. Fujimoto et al.[27] computed elastic DCSs and ICSs for low-energy electron collisions using the R-matrix method including the polarization effects of long-range dipole

TABLE I. Present experimental DCSs, ICSs, and MTCSs for elastic electron scattering from acetonitrile. DCSs are in units of 10^{-16} cm^2/sr, and ICSs and MTCSs are in units of 10^{-16} cm^2. Errors include uncertainties in the helium elastic DCSs, uncertainties in flow rates, statistical uncertainties, and standard deviation uncertainties of multiple DCSs measurements. See text for discussion.

Angle (deg)	0.7 eV	Error	1 eV	Error	2 eV	Error	4 eV	Error	5 eV	Error
15									41.1	7.1
20					69.5	10.3	31.8	5.2	33.3	4.5
25	86.8	13.5	86.0	16.5	44.8	5.9	18.3	2.5	19.3	2.7
30	70.1	9.3	53.8	7.0	32.3	4.2	12.0	1.5	11.9	1.6
35	57.3	7.6								
40	45.8	6.3	29.0	3.9	14.9	1.8	5.59	0.72	5.52	0.70
50	21.5	2.6	14.1	1.9	7.08	0.91	3.39	0.43	3.10	0.40
60	13.5	1.7	8.05	1.06	4.12	0.52	3.09	0.39	2.76	0.32
70	8.08	1.11	4.90	0.65	3.57	0.46	2.92	0.36	2.83	0.34
80	5.95	0.80	3.42	0.45	2.80	0.36	3.03	0.37	2.95	0.36
90	3.94	0.52	2.41	0.31	2.47	0.31	2.72	0.33	2.66	0.30
100	2.78	0.36	2.00	0.27	2.22	0.27	2.42	0.30	2.27	0.26
110	2.20	0.30	1.83	0.24	1.75	0.22	2.25	0.28	1.86	0.21
120	1.88	0.25	1.71	0.23	1.54	0.19	1.89	0.23	1.68	0.21
125	1.79	0.24								
130			1.54	0.20	1.35	0.17	2.02	0.25	1.77	0.23
ICS	199	36	145	26	99.2	16.7	66.9	11.8	58.6	8.4
MTCS	59.6	8.1	41.9	5.6	31.2	4.0	32.1	4.1	29.0	3.6

Angle (deg)	7 eV	Error	10 eV	Error	15 eV	Error	20 eV	Error	30 eV	Error
10									52.6	6.7
15	40.9	6.8	36.5	4.9	26.0	4.1	39.5	4.9	23.6	3.2
20	23.8	3.2	22.0	2.8	14.9	1.7	20.2	2.3	11.8	1.5
25	14.9	1.9	13.6	1.7	10.6	1.2	11.2	1.4	6.27	0.77
30	10.0	1.3	9.42	1.19	7.67	0.93	7.29	0.93	3.27	0.41
40	4.79	0.63	5.43	0.65	3.84	0.46	3.57	0.45	1.63	0.20
50	3.15	0.43	3.45	0.40	2.62	0.32	2.22	0.27	0.990	0.119
60	2.63	0.33	2.61	0.33	1.95	0.25	1.65	0.21	0.653	0.077
70	2.72	0.35	2.26	0.28	1.36	0.17	1.00	0.12	0.388	0.050
80	2.62	0.34	1.92	0.24	1.05	0.12	0.731	0.089	0.334	0.045
90	2.18	0.28	1.64	0.21	0.938	0.112	0.770	0.093	0.244	0.033
100	1.93	0.25	1.51	0.19	0.981	0.123	0.727	0.091	0.226	0.030
110	1.65	0.21	1.36	0.17	0.955	0.128	0.767	0.098	0.321	0.043
120	1.63	0.20	1.36	0.17	1.00	0.13	0.734	0.093	0.405	0.054
130	1.67	0.21	1.51	0.19	1.16	0.14	0.920	0.114	0.518	0.070
ICS	54.2	7.9	50.0	7.0	35.9	5.1	38.9	5.9	23.9	3.4
MTCS	26.4	3.4	23.6	3.0	16.8	2.2	14.2	2.0	6.97	1.07

interactions. For DCSs, they used the static exchange plus polarization (SEP) model, including the Born correction. On the other hand, Maioli and Bettega[26] provided the calculations of DCSs and ICSs employing the SMC method implemented with norm conserving pseudopotentials and also obtained the DCSs and ICSs which included Born corrections for polarization. In Fig. 2, the SMC DCSs computed using their SEP code are plotted, together with the R-matrix code of Fujimoto et al.[27]

At lower E_0 values (1 eV, 2 eV), our experimental DCSs are found to lie between the two theoretical models with a better shape agreement with the SMC than with the R-matrix. However, for angles <40°, the agreement is better with the R-matrix model than with the SMC approach. At E_0 values of 4–10 eV, the agreement between the measured acetonitrile DCSs improves especially with the R-matrix method, over a wide range of angles. Overall there is a good qualitative agreement between the SMC calculation and the present experiment. Especially for energies 4-7 eV, we can observe an interesting broad enhancement in DCSs ranging from 60° to 120°, both in the experimental and SMC calculation results. At 15 and 20 eV, the calculated SMC DCSs agree very well with the experiment. It has been previously observed that the SMC approach predicts higher value DCSs above the ionization energy because of flux coming from the ionization reactions.[35,36] As expected, the angular distribution shows enhanced forward scattering for all measured energies, typical for molecules that possess large permanent dipole moments, and so our experimental DCSs rise steeply due to this long-range scattering by the dipole electric field of acetonitrile.
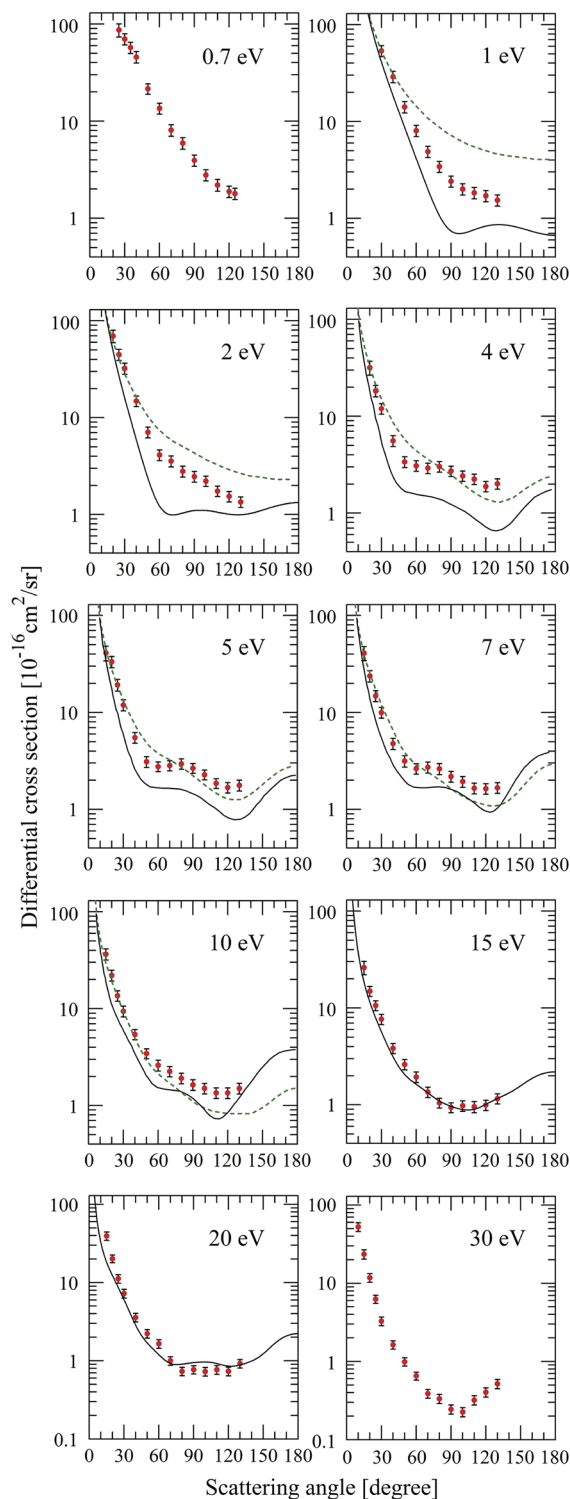
FIG. 2. Present elastic scattering DCSs at different E_0 values (red dots). We compare our DCSs with the calculations of Maioli and Bettega[26] (solid black line) and Fujimoto et al.[27] (dashed green line). See text for discussion.

FIG. 3. ICSs for elastic electron scattering by acetonitrile. The available theoretical data of the R-matrix[27] and the SMC[26] models with different approximations are also plotted (see the legend in the figure).

structure is shifted to around 2.22 eV while applying the SEP approach. A similar feature peaking at 2.4 eV is observed by Fujimoto et al.[27] when applying the SEP approximation without Born corrections. This resonance is assigned to electron capture into the degenerate π^* molecular orbital, a process which was also probed by Hitchcock et al.[15] in electron transmission spectroscopy, which resulted in an attachment energy for acetonitrile at 2.82 eV for this orbital. They also showed two weaker resonances in their electron transmission spectrum around 5.7 and 6.8 eV;[15] however, we cannot confirm these using our present results. These structures are claimed to originate from electron capture into σ^* molecular orbitals or core-excited shape resonances. Edard et al.[17] also showed the existence of two shape resonances around 2.9 eV and 5.8 eV. Jordan and Burrow[18] observed a π^* resonance near 2.8 eV using electron transmission spectroscopy. It is seen in Fig. 3, depending on the approximation applied, that there is a large quantitative spreading of the theoretical ICS data. For molecules like acetonitrile, one needs to include the dipole field interaction to correctly describe processes taking place when the electrons interact with the molecule. However this low-energy dominant process is difficult to predict accurately[37] due to the almost singular behavior of the DCSs at small θ. For the two different models that are considered here, the present ICSs show poor quantitative agreement between the models. Present experimental ICS data show poor agreement for energies <4 eV with the SMC method. At higher E_0, we can also observe a possible improvement regarding any quantitative agreement with the SMC model.

In Fig. 4, we present MTCSs determined from experimental data in the $E_0 = 0.7$–30 eV range. We have also evaluated MTCSs from integrating the theoretical DCSs, derived from digitizing their graphs or from supplied tables.[38] These MTCSs are shown in Fig. 4. We note here that unlike the ICSs, the MTCSs are not as affected by forward scattering and offer better comparison with theory for dipole scattering systems. Interestingly, the MTCS shows a possible enhancement centered between 2 and 4 eV. This resonant structure can be associated with a π^* anti-bonding shape resonance.[17] Our results are also in good agreement with the production of negative fragment ions at around 3 eV.[20,21] In dissociative electron

Maioli and Bettega[26] have computed ICSs in their static-exchange (SE) and static-exchange plus polarization (SEP) approximations, with and without the inclusion of the Born-closure procedure. For the ICS computations, Fujimoto et al.[27] used their SEP model, with and without Born corrections (see Fig. 3). According to Maioli and Bettega,[26] their SE cross sections display a π^* resonance around 4.6 eV. This resonance
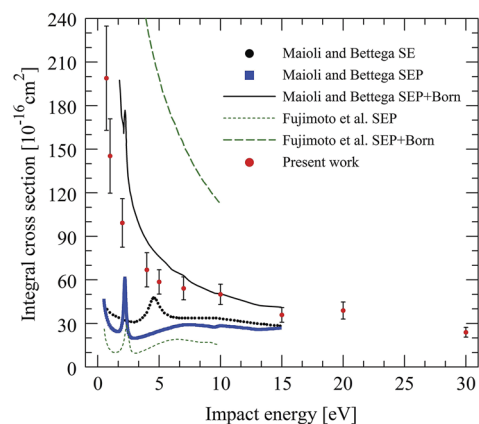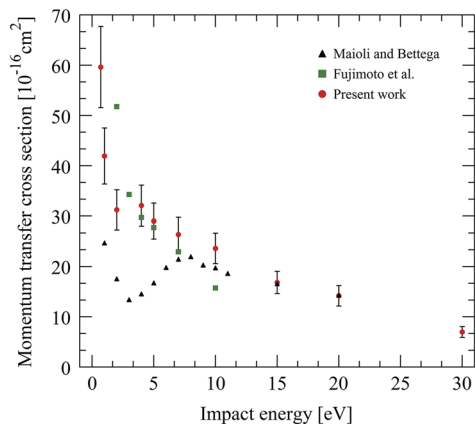
FIG. 4. MTCSs for elastic electron scattering by acetonitrile. See text for discussion.

attachment studies, the most intense fragment ion formed is CH_2CN^- from the fragmentation of the parent anion by the loss of a single hydrogen atom. Its appearance energy was estimated theoretically as 2.44 ± 0.20 eV with the reported experimental value of 2.35 ± 0.10 eV.[21] The maximum cross section for the production of CH_2CN^- peaks at 3.2 eV. This suggests that the detected π^* resonance observed in the present studies decays by a dissociative decay channel.

IV. CONCLUSIONS

We have reported experimental differential elastic scattering cross sections for acetonitrile over a wide range of E_0 (0.7–30 eV) and θ (10°–130°). Comparisons with the available R-matrix and SMC-SEP-Born level calculations were made. Agreement for energies less than about 15 eV was found to be unsatisfactory and needs to be improved; however, the R-matrix method was quantitatively closer to our measured values. On the other hand, the SMC approach reasonably predicted qualitative trends of our DCSs. For energies ≥15 eV, we notice some improvement in agreement with the SMC method. Additionally, for a molecule having a large dipole moment, the present data show clear evidence for the effect of this dipole scattering. Furthermore, DCS values have been used to calculate the integral and momentum-transfer cross sections, depicting a π^* resonance located around 3 eV. This resonant feature is not observed in any of the calculations. These measurements also provide important experimental data in the literature for the improvement of theoretical models for this important target. It is hoped that future models will provide for such an improvement of theoretical models for acetonitrile.

ACKNOWLEDGMENTS

[1] I. I. Fabrikant, S. Eden, N. J. Mason, and J. Fedor, Adv. At., Mol., Opt. Phys. **66**, 545 (2017).
[2] I. Baccarelli, I. Bald, F. A. Gianturco, E. Illenberger, and J. Kopyra, Phys. Rep. **508**, 1 (2011).
[3] R. K. Janev, *Atomic and Molecular Processes in Fusion Edge Plasmas* (Plenum, New York, 1995).
[4] G. Karwasz and K. Fedus, Fusion Sci. Technol. **63**, 338 (2013).
[5] J. Lengyel, M. Ončák, J. Fedor, J. Kočišek, A. Pysanenko, M. K. Beyer, and M. Fárnik, Phys. Chem. Chem. Phys. **19**, 11753 (2017).
[6] J. Kočišek, R. Janečková, and J. Fedor, J. Chem. Phys. **148**, 074303 (2018).
[7] M. J. Frisch *et al.*, GAUSSIAN 09, Revision E.01, Gaussian, Inc., Wallingford, CT, 2009.
[8] R. J. Habing and G. H. Macdonald, Astron. Astrophys. **252**, 705 (1991).
[9] A. Coustenis, B. Schmitt, R. K. Khanna, and F. Trotta, Planet. Space Sci. **47**, 1305 (1999).
[10] C. Watson, E. Churchwell, V. Pankonin, and J. H. Bieging, Astrophys. J. **577**, 260 (2002).
[11] R. B. Loren and L. G. Mundy, Astrophys. J. **286**, 232 (1984).
[12] P. Hofner, S. Kurtz, E. Churchwell, C. M. Walmsley, and R. Cesaroni, Astrophys. J. **460**, 359 (1996).
[13] V. Pankonin, E. Churchwell, C. Watson, and J. H. Bieging, Astrophys. J. **558**, 194 (2001).
[14] M. B. Robin, *Higher Excited States of Polyatomic Molecules* (Academic, New York, 1974), Vols. I and II; 1986, Vol. III.
[15] A. P. Hitchcock, M. Tronc, and A. Modelli, J. Phys. Chem. **93**, 3068 (1989).
[16] F. Edard and M. Tronc, J. Phys. B: At. Mol. Phys. **20**, L265 (1987).
[17] F. Edard, A. P. Hitchcock, and M. Tronc, J. Phys. Chem. **94**, 2768 (1990).
[18] K. D. Jordan and P. D. Burrow, Acc. Chem. Res. **11**, 341 (1978).
[19] M. Ben Arfa and M. Tronc, J. Electron Spectrosc. Relat. Phenom. **50**, 117 (1990).
[20] M. Heni and E. Illenberger, Int. J. Mass Spetrosc. Ion Processes **73**, 127 (1986).
[21] W. Sailer, A. Pelc, P. Limao-Vieira, N. J. Mason, J. Limtrakul, P. Scheier, M. Probst, and T. D. Meark, Chem. Phys. Lett. **381**, 216 (2003).
[22] P. A. Steiner and W. Gordy, J. Mol. Spectrosc. **21**, 291 (1966).
[23] I. I. Fabrikant, J. Phys. B: At., Mol. Opt. Phys. **49**, 222005 (2016).
[24] G. A. Gallup, P. Burrow, and I. Fabrikant, Phys. Rev. A **79**, 042701 (2009).
[25] M. Zawadzki, M. Ranković, J. Kočišek, and J. Fedor, Phys. Chem. Chem. Phys. **20**, 6838 (2018).
[26] L. S. Maioli and M. H. F. Bettega, Eur. Phys. J. D **71**, 322 (2017).
[27] M. M. Fujimoto, E. V. R. de Lima, and J. Tennyson, Eur. Phys. J. D **69**, 153 (2015).
[28] M. A. Khakoo, C. E. Beckmann, S. Trajmar, and G. Csanak, J. Phys. B: At. Mol. Phys. **27**, 3159 (1994).
[29] ARi Industries, Inc., Addison, IL 60101, USA, 1HN040B-16.3 biaxial cable.
[30] ETP Equipe Thermodynamique et Plasmas (ETP) model AF151.
[31] M. A. Khakoo, J. Blumer, K. Keane, C. Campbell, H. Silva, M. C. A. Lopes, C. Winstead, V. McKoy, R. F. da Costa, L. G. Ferreira, M. A. P. Lima, and M. H. F. Bettega, Phys. Rev. A **77**, 042705 (2008).
[32] M. Hughes, K. E. James, Jr., J. G. Childers, and M. A. Khakoo, Meas. Sci. Technol. **14**, 841 (2003).
[33] R. K. Nesbet, Phys. Rev. A **20**, 58 (1979).
[34] D. F. Register, S. Trajmar, and S. K. Srivastava, Phys. Rev. A **21**, 1134 (1980).
[35] M. A. Khakoo, K. Keane, C. Campbell, N. Guzman, and K. Hazlett, J. Phys. B: At., Mol. Opt. Phys. **40**, 3601 (2007).
[36] A. Sakaamini, C. Navarro, J. Cross, L. R. Hargreaves, M. A. Khakoo, K. Fedus, C. Winstead, and V. McKoy, J. Phys. B: At., Mol. Opt. Phys. **48**, 205202 (2015).
[37] M. A. Khakoo, H. Silva, J. Muse, M. C. A. Lopes, C. Winstead, and V. McKoy, Phys. Rev. A **78**, 052710 (2008).
[38] L. S. Maioli and M. H. F. Bettega, private communications (2018).